# Petrology and Mineral Chemistry of a Porphyritic Mafic Dyke, Jonnagiri Schist Belt, Eastern Dharwar Craton, India: Implications for Its Magmatic Origin


**V. V. Sesha Sai, S. N. Mahapatro, Santanu Bhattacharjee, Tarun C. Khanna and M. M. Korakoppa**

**Abstract** We present field, petrology and mineralogy of a porphyritic mafic dyke that traverses the granite-greenstone terrain of the Neoarchean Jonnagiri schist belt, eastern Dharwar craton, India. The undeformed porphyritic dyke is characterised by the presence of euhedral plagioclase megacrysts (0.5–3.5 cm) exhibiting primary magmatic alignment. At places, partial resorption is noticed in the plagioclase phenocrysts indicating crystal-melt interaction. The groundmass consists of andesine and titan augite. Sub-ophitic/ophitic textures are conspicuously noticed. Ilmenite, titano-magnetite, apatite and baddeleyite are the accessory phases. Exsolved ilmenite and titano-magnetite along with euhedral apatite is also observed in the porphyritic dyke. Mineral chemistry of plagioclase shows variation between $Or_{3.50–6.44\%}$, $Ab_{43.18–62.98\%}$ and $An_{30.57–52.46\%}$. Clustering of biotite, is noticed at places. EPMA analyses of plagioclase reveals the presence of normal zoning; $Ab_{45.73}$ in the core to $Ab_{49.61}$ in the rim. The predominantly andesine composition of plagioclase, position of clinopyroxene in the Ca + Na versus Ti binary mineral chemistry diagram, and the micron size euhedral baddeleyite indicate transitional nature of the Jonnagiri porphyritic

V. V. Sesha Sai (✉) · S. Bhattacharjee · M. M. Korakoppa
Geological Survey of India, Bandlaguda, Hyderabad, India
e-mail: seshu1967@gmail.com

S. Bhattacharjee
e-mail: bhattacharjeesantanu21@gmail.com

M. M. Korakoppa
e-mail: korakoppam@gmail.com

S. N. Mahapatro
Geological Survey of India, Central Region, Raipur, India
e-mail: snmahagsi@gmail.com

T. C. Khanna
CSIR-National Geophysical Research Institute, Habsiguda, Hyderabad, India
e-mail: khannangri@ngri.res.in



R. K. Srivastava et al. (eds.), *Dyke Swarms of the World: A Modern Perspective*,
Springer Geology, https://doi.org/10.1007/978-981-13-1666-1_10

dyke. The clinopyroxene is compositionally a Ti-augite ($Wo_{40}En_{34}Fs_{26}$). The temperature and oxygen fugacity estimates for the coexisting magnetite-ilmenite solid solution pair yielded an equilibration temperature of ~756 °C and $10^{-15.6}$atm$f_{O2}$ for the Jonnagiri porphyritic dyke.

**Keywords** Mafic dyke · Porphyritic · Magmatic origin · Jonnagiri belt
Eastern Dharwar craton · India

## 1 Introduction

Emplacement of dyke swarms in a shield area provide critical information on the palaeocontinental reconstruction (e.g. Hou et al. 2008; Zhao et al. 2004; Santosh 2012), and, therefore, a key for geodynamic interpretation (Srivastava 2011). The Indian shield has recorded extensive activity of mafic magmatism (e.g. Naqvi and Rogers 1987; Srivastava et al. 2008; Srivastava and Ahmed 2009; Srivastava 2011; Srivastava et al. 2015). The granite-greenstone terrain of the Dharwar craton, the Proterozoic Cuddapah basin, and the high-grade granulite belt in the southern part of Indian shield, witnessed extensive dyke and sill intrusions, particularly during Paleoproterozoic (e.g. Radhakrishna and Joseph 1996; Halls et al. 2007; Radhakrishna 2008; Jayananda et al. 2008; Srivastava 2011; Kumar et al. 2012, 2015; Khanna et al. 2013; Belica et al. 2013; Srivastava et al. 2014a, b, 2015; Sesha Sai et al. 2017). Chronologically, two distinct phases (~2370 and ~1890 Ma) of dyke swarms in the Dharwar craton, which predominantly trend in east-west direction, have been identified (Piispa et al. 2011; Srivastava et al. 2014a, c, 2015). Additionally, two other dyke swarms, emplaced at ~2.21 and ~2.18 Ga, have also recorded from the eastern Dharwar craton (Srivastava et al. 2015). Recently, Kumar et al. (2015) have reported ~2.08 Ga mafic dyke swarm in the eastern Dharwar craton (EDC). Although, plagioclase megacryst bearing dykes are pervasively noticed as large swarms in many granite-greenstone terrains in the Archean shield areas (e.g. Phinney and Morrison 1986; Morrison et al. 1988), mafic dyke(s) with plagioclase megacrysts are less known from the Dharwar craton. Plagioclase megacrysts bearing leuco-gabbronorite dyke have been reported from the Bastar craton (Dora et al. 2016).

## 2 Geological Setting

The Jonnagiri schist belt (JSB) is located close to the vicinity of the western margin of the Proterozoic Cuddapah basin in the EDC, Southern India. The northern part of the schist belt is of 11 km long and up to 5 km wide and exposed in sigmoid shape trending WNW–ESE. In the southeastern part, it abruptly changes into a linear band of about 0.8 km width, trending NNW–ESE to NNE–SSW for a length of 16 km from Aminabad to Gooty (Sreeramachandra Rao et al. 2001). WNW–ESE trending mafic

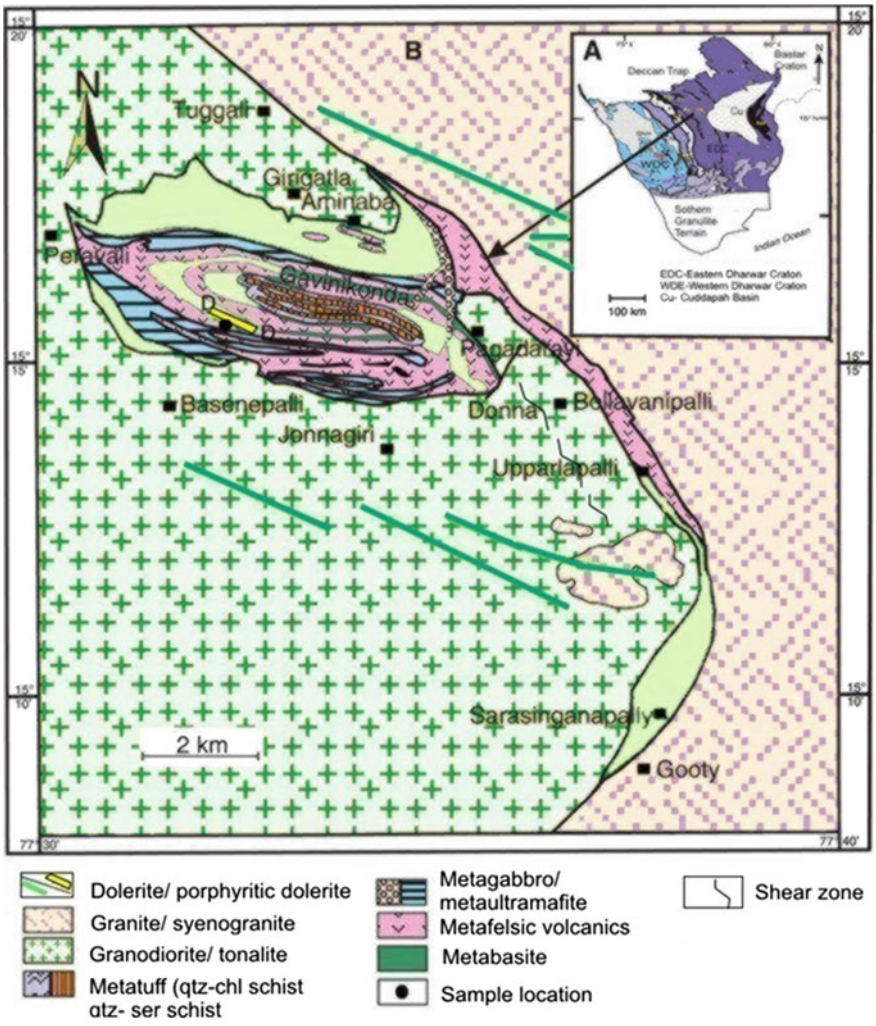


**Fig. 1** Geological map of Jonnagiri and adjoining areas, Eastern Dharwar Craton, India (Modified after Jairam et al. 2001). Inset map showing the location of the JSB close the western margin of the Proterozoic Cuddapah basin

dykes of Proterozoic age have been recorded within the granite-greenstone terrain around Jonnagiri area in the EDC (e.g. Jairam et al. 2001). This belt represents the Jonnagiri shear zone which is traceable for 25 km further south-southwest up to Julakalva schist belt near the border of Proterozoic Cuddapah Basin. The belt lies between 15°05′ and 15°20′ latitudes and 77°30′ and 77°40′ longitudes.

Lithologically, the JSB is comprised of metamorphosed basic and acid volcanic together with tuffaceous rocks in the form of quartz sericite schist and sericite-

**Fig. 2** Field photograph showing plagioclase phenocrysts in the Jonnagiri porphyritic dyke. Note the alignment in larger plagioclase phenocrysts

chlorite schist and ultramafite. Geological Survey of India carried out studies on the granitoids of the Peninsular Gneissic Complex (PGC) in the Gooty-Singanamala area (Suresh and Viswanatha Rao 1994); specialised thematic mapping in the areas comprising the southern extension of JSB and Julakalva schist belt in EDC (Suresh and Jaiswal 2003). The metabasalts of the Neoarchaean JSB exhibit 'arc—nascent back—arc signatures' (Manikyamba et al. 2015).

The JSB has been subjected to a number of phases of deformation and is intruded by younger granitoids and dolerite dykes, while undeformed dolerite dykes (porphyritic) of Proterozoic age are noticed in and around the JSB (e.g., Sreeramachandra Rao et al. 2001; Jairam et al. 2001). The present paper deals with the field, petrological and mineral chemistry studies of a major WNW–ESE trending porphyritic mafic dyke emplaced in the granite-greenstone terrain of the JSB, EDC, India; located within the folded metavolcanic sequence of the JSB and lies between Pagadarayi and Peravali (Fig. 1). Field observations indicate that the dyke is intermittently exposed over a stretch of >2 km as low-lying outcrops striking in WNW–ESE direction. The size of the plagioclase megacrysts ranges from 0.5 cm to a maximum of 7 cm in diameter. The dyke is undeformed and is characterised by the presence of aligned large megacrysts of plagioclase (Fig. 2). The euhedral nature of the phenocrysts and preservation of terminal ends in some of the plagioclase phenocrysts indicate

that the alignment of plagioclase phenocrysts is magmatic. Phenocryst groundmass ration varies from 15 (phenocryst): 85 (groundmass) in the peripheral part to 30 (phenocryst): 70 (groundmass) in the central part of the porphyritic dyke. Partial resorption is some plagioclase phenocryst indicate crystal-melt interaction.

## 3 Methodology

Samples were collected during the course of field studies. Based on megascopic observations, 15 representative samples have been selected from the Jonnagiri porphyritic dyke for preparation of thin cum polished sections. Mineral chemistry was determined by EPMA, Petrology Division, GSI, SR, Hyderabad by CAMECA SX 100. Analyses conditions: Accelerating voltage: 15 kV, current: 15 nA. Beam size: 1 μm. Signal used Na Ka, Mg Ka, Al Ka, K Ka, Cr Ka, Mn Ka, Fe Ka, P Ka, Ni Ka, Zr La, Ca Ka, Ti K. All natural standards have been used except for Mn and Ti for which synthetic standards have been used.

## 4 Petrography and Mineral Chemistry

Petrographic studies reveal that the dyke exhibits porphyritic texture and essentially composed of plagioclase and clinopyroxene, while apatite is noticed as a conspicuous accessory mineral. Large euhedral phenocrysts of plagioclase (Fig. 3a) are embedded in subhedral grains of clinopyroxene and groundmass plagioclase. Sub-ophitic texture is conspicuously noticed in these samples, wherein plagioclase is partially enclosed in clinopyroxene (Fig. 3b).

At places, ophitic texture is also noticed (Fig. 3c). Opaque phases are mostly confined to the clinopyroxene (Fig. 3d). At places, it is observed that euhedral to subhedral opaques are partially enclosed in clinopyroxene (Fig. 3e). It is also noticed that partially enclosed opaque in ophitic plagioclase within the clinopyroxene (Fig. 3f). Megascopic studies show that the relatively large plagioclase phenocrysts show alignment at places. Microscopic studies of the plagioclase in the groundmass of Jonnagiri porphyritic dyke indicate the presence of randomly oriented plagioclase laths. At places, it is noticed that the plagioclase is altered along the margins. Mineral chemistry studies indicate the presence of euhedral baddeleyite. EPMA analyses have been carried out by selecting areas in plagioclase that are fresh and unaltered.

Presence of greenish amphibole and minor amounts of biotite, after alteration of the clinopyroxene is also noticed in the Jonnagiri porphyritic dyke. Opaques are represented by Fe–Ti oxides i.e. ilmenite and titano-magnetite. Jonnagiri porphyritic dyke is characterized by the presence of both apatite and Fe–Ti oxides. Both ilmenite and magnetite together constitute about ~10% in the rock are noticed as subhedral to euhedral grains that are more or less uniformly distributed in the rock. Apatite is noticed as minute euhedral inclusion in clinopyroxene. The petrographic obser-

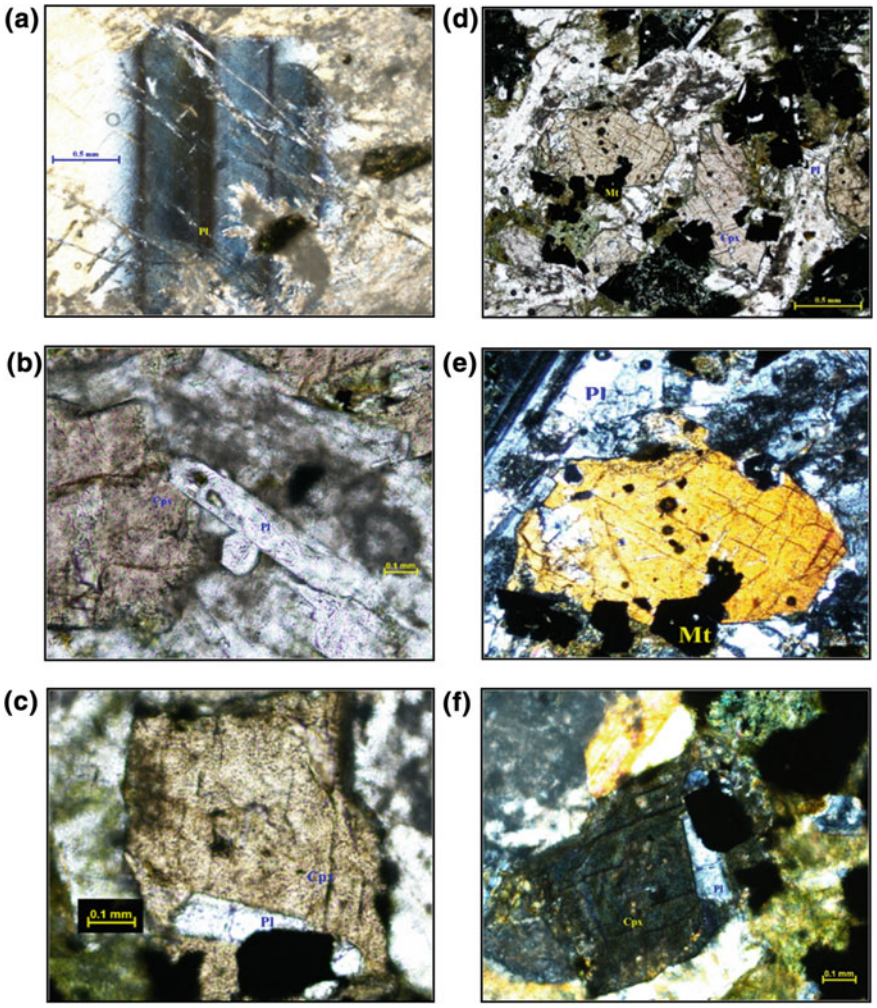


**Fig. 3** **a** Plagioclase phenocryst in Xed. **b** Sub-ophitic texture in PPL. **c** Ophitic texture in PPL. **d** Opaques in clinopyroxene (Cpx) PPL. **e** Opaques in clinopyroxene Xed. Note the lamellar twining in plagioclase (Pl), and **f** Photomicrograph in Xed showing partially enclosed opaque in ophitic plagioclase within the clinopyroxene

vations are substantiated by SEM images (Fig. 4a–c), while the EPMA analyses of the plagioclase and pyroxene have been plotted in the respective mineral chemistry diagrams (Figs. 5 and 6). The EPMA analyses of the pyroxene from the Jonnagiri porphyritic dyke has been plotted in the Ca + Na versus Ti binary mineral chemistry diagram for pyroxene (Fig. 7; after Leterrier et al. 1982) which indicate the transitional nature of the Jonnagiri porphyritic dyke. Small grains of euhedral baddeleyite are also observed (Fig. 8).

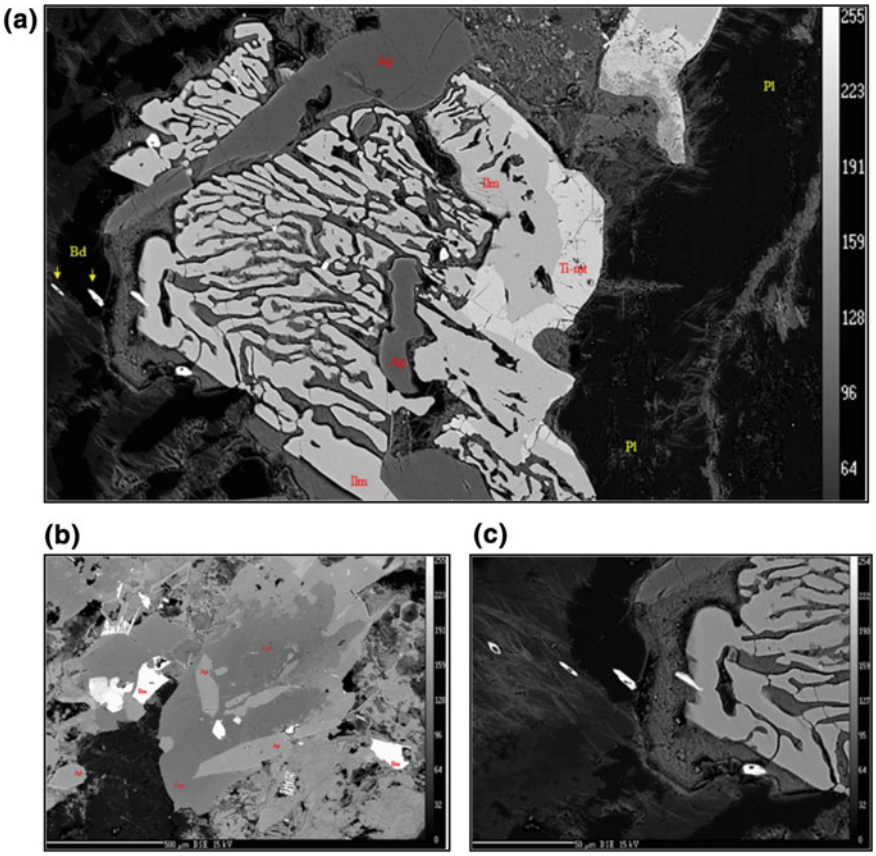


**Fig. 4** **a** BSE image showing exsolved ilmenite and titano-magnetite along with apatite in the porphyritic dyke. Note that the titano-magnetite occurs at the rim and ilmenite in the core, **b** BSE image showing euhedral apatite inclusions within the clinopyroxene in Jonnagiri porphyritic dyke, and **c** BSE image showing the oriented baddeleyite grains ranging in size from 10 to 12 μm. Note that one of the baddeleyite grain partially transects the ilmenite

## *4.1 Plagioclase*

Plagioclase occurs large size phenocrysts as well as relatively fine-grained laths in groundmass. Under crossed-nicols, it exhibits characteristic lamellar twining (Figs. 3a, e). EPMA analyses of plagioclase grains indicate that $SiO_2$ range from 53.90 to 58.34%, $Al_2O_3$ from 23.92 to 27.24%, CaO contents range from 7.49 to 10.04% and $Na_2O$ contents from 4.82 to 7.09%. $K_2O$ content of 0.61 to 1.24%. Zoning is noticed in plagioclase.

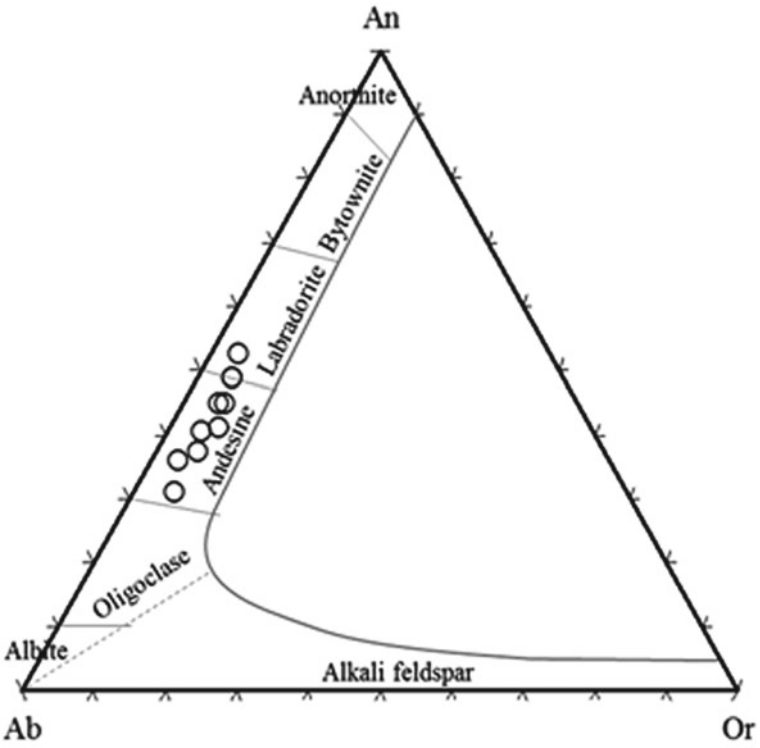


**Fig. 5** Orthoclase (Or)—Albite (Ab)—Anorthite (An) ternary mineral chemistry diagram showing the position of plagioclases

End member calculation from the EPMA analytical data of plagioclases suggest their compositional variation from orthoclase$_{3.50–6.44\%}$, albite$_{43.18–62.98\%}$ to anorthite$_{30.57–52.46\%}$. On the Orthoclase (Or)—Albite (Ab)—Anorthite (An) ternary mineral chemistry diagram, analyses of the plagioclase core in the phenocrysts indicate labradorite composition, while the analyses of plagioclase rim in phenocrysts as well as groundmass plagioclase of the Jonnagiri porphyritic dyke falls in the field of andesine (Fig. 5). The andesine to labradorite composition of the plagioclase in Jonnagiri dyke, perhaps indicate relatively less density of the plagioclase than the basaltic magma from which it crystallised.

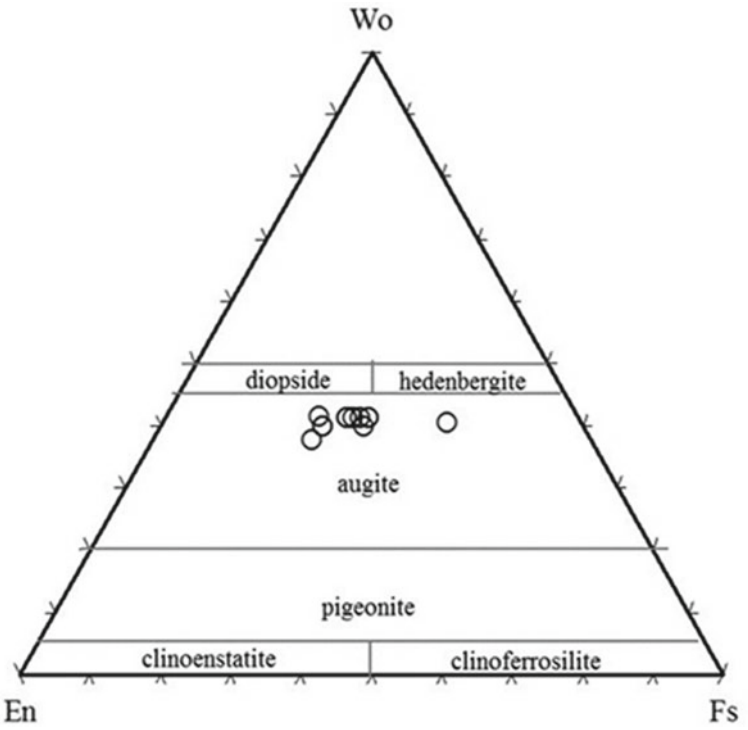


**Fig. 6** Wollastonite (Wo)—Enstatite (En)—Ferrosilite (Fs) mineral chemistry ternary diagram showing position of pyroxenes

Further, predominant andesine composition indicates its relatively alkaline nature suggesting emplacement in a crustally thinned tectonic domain (e.g. Khanna et al. 2013). The mineral chemistry of the plagioclase feldspar from the Jonnagiri porphyritic dyke is presented in Table 1.

## *4.2 Clinopyroxene*

Clinopyroxene occurs as euhedral to subhedral grains showing moderate relief and well-developed cleavage in plane polarised light (Fig. 3d), while in crossed nicols it is anisotropic, exhibits inclined extinction and second order interference colours (Fig. 3e). It is usually noticed as an intergranular phase in between lath shaped plagioclase.

EPMA analyses of the clinopyroxene indicate a relatively lower $SiO_2$ content (<50%). $SiO_2$ contents in the clinopyroxene range from 48.08 to 49.82%. $TiO_2$ contents in clinopyroxene range from 0.74 to 1.33%, while $Al_2O_3$ ranges from 0.35 to

**Table 1** Mineral chemistry of plagioclase from the porphyritic dyke, Jonnagiri schist belt, EDC, India

| | 1 | 2 | 17 | 18 | 19 | 20 | 31 | 32 | 33 | 34 |
|---|---|---|---|---|---|---|---|---|---|---|
| $SiO_2$ | 55.400 | 56.828 | 53.904 | 57.032 | 54.410 | 57.014 | 57.678 | 58.348 | 55.941 | 59.241 |
| $TiO_2$ | 0.156 | 0.004 | 0.104 | 0.096 | 0.089 | 0.063 | 0.108 | 0.168 | 0.094 | 0.081 |
| $Al_2O_3$ | 27.246 | 26.443 | 27.234 | 25.469 | 26.863 | 25.648 | 25.031 | 25.040 | 26.219 | 23.925 |
| $Cr_2O_3$ | 0.000 | 0.000 | 0.015 | 0.000 | 0.003 | 0.001 | 0.010 | 0.013 | 0.001 | 0.000 |
| FeOT | 0.580 | 0.533 | 0.429 | 0.414 | 0.511 | 0.520 | 0.446 | 0.681 | 0.537 | 0.475 |
| MnO | 0.000 | 0.030 | 0.045 | 0.099 | 0.028 | 0.000 | 0.041 | 0.000 | 0.000 | 0.031 |
| MgO | 0.063 | 0.047 | 0.066 | 0.054 | 0.061 | 0.056 | 0.027 | 0.014 | 0.053 | 0.027 |
| CaO | 10.012 | 9.328 | 10.602 | 8.276 | 10.046 | 8.471 | 7.498 | 7.542 | 9.308 | 6.227 |
| $Na_2O$ | 5.162 | 5.642 | 4.823 | 6.193 | 5.289 | 5.873 | 6.310 | 6.887 | 5.594 | 7.090 |
| $K_2O$ | 0.900 | 0.868 | 0.738 | 0.921 | 0.864 | 1.249 | 1.090 | 0.611 | 1.041 | 1.102 |
| NiO | 0.082 | 0.000 | 0.148 | 0.088 | 0.031 | 0.061 | 0.000 | 0.005 | 0.000 | 0.000 |
| Total | 99.601 | 99.723 | 98.107 | 98.642 | 98.212 | 98.960 | 98.249 | 99.309 | 98.820 | 98.199 |
| $Fe_2O_3$ | 0.269 | 0.000 | 0.334 | 0.414 | 0.511 | 0.520 | 0.000 | 0.681 | 0.537 | 0.132 |
| FeO | 0.338 | 0.533 | 0.128 | 0.000 | 0.000 | 0.000 | 0.446 | 0.000 | 0.000 | 0.356 |
| Total | 99.628 | 99.723 | 98.141 | 98.642 | 98.195 | 98.956 | 98.239 | 99.309 | 98.788 | 98.212 |
| Cations: | 8(O) | 8(O) | 8(O) | 8(O) | 8(O) | 8(O) | 8(O) | 8(O) | 8(O) | 8(O) |
| Si | 2.514 | 2.569 | 2.487 | 2.601 | 2.507 | 2.595 | 2.635 | 2.635 | 2.555 | 2.698 |
| Ti | 0.005 | 0.000 | 0.004 | 0.003 | 0.003 | 0.002 | 0.004 | 0.006 | 0.003 | 0.003 |

(continued)

**Table 1** (continued)

| | 1 | 2 | 17 | 18 | 19 | 20 | 31 | 32 | 33 | 34 |
|---|---|---|---|---|---|---|---|---|---|---|
| Al | 1.458 | 1.409 | 1.481 | 1.369 | 1.459 | 1.376 | 1.348 | 1.333 | 1.412 | 1.284 |
| $Fe^{+3}$ | 0.009 | 0.000 | 0.012 | 0.014 | 0.018 | 0.018 | 0.000 | 0.023 | 0.018 | 0.005 |
| $Fe^{+2}$ | 0.013 | 0.020 | 0.005 | 0.000 | 0.000 | 0.000 | 0.017 | 0.000 | 0.000 | 0.014 |
| Mn | 0.000 | 0.001 | 0.002 | 0.004 | 0.001 | 0.000 | 0.002 | 0.000 | 0.000 | 0.001 |
| Mg | 0.004 | 0.003 | 0.005 | 0.004 | 0.004 | 0.004 | 0.002 | 0.001 | 0.004 | 0.002 |
| Ca | 0.487 | 0.452 | 0.524 | 0.404 | 0.496 | 0.413 | 0.367 | 0.365 | 0.456 | 0.304 |
| Na | 0.454 | 0.495 | 0.432 | 0.548 | 0.473 | 0.518 | 0.559 | 0.603 | 0.495 | 0.626 |
| K | 0.052 | 0.050 | 0.043 | 0.054 | 0.051 | 0.073 | 0.064 | 0.035 | 0.061 | 0.064 |
| Ni | 0.003 | 0.000 | 0.005 | 0.003 | 0.001 | 0.002 | 0.000 | 0.000 | 0.000 | 0.000 |
| Total | 5.000 | 4.999 | 5.000 | 5.004 | 5.013 | 5.001 | 4.998 | 5.001 | 5.004 | 5.000 |
| Orthoclase | 5.247 | 5.024 | 4.348 | 5.329 | 4.983 | 7.224 | 6.420 | 3.509 | 5.996 | 6.442 |
| Albite | 45.735 | 49.631 | 43.189 | 54.457 | 46.358 | 51.627 | 56.488 | 60.113 | 48.973 | 62.988 |
| Anorthite | 49.019 | 45.345 | 52.463 | 40.215 | 48.659 | 41.149 | 37.092 | 36.378 | 45.030 | 30.571 |

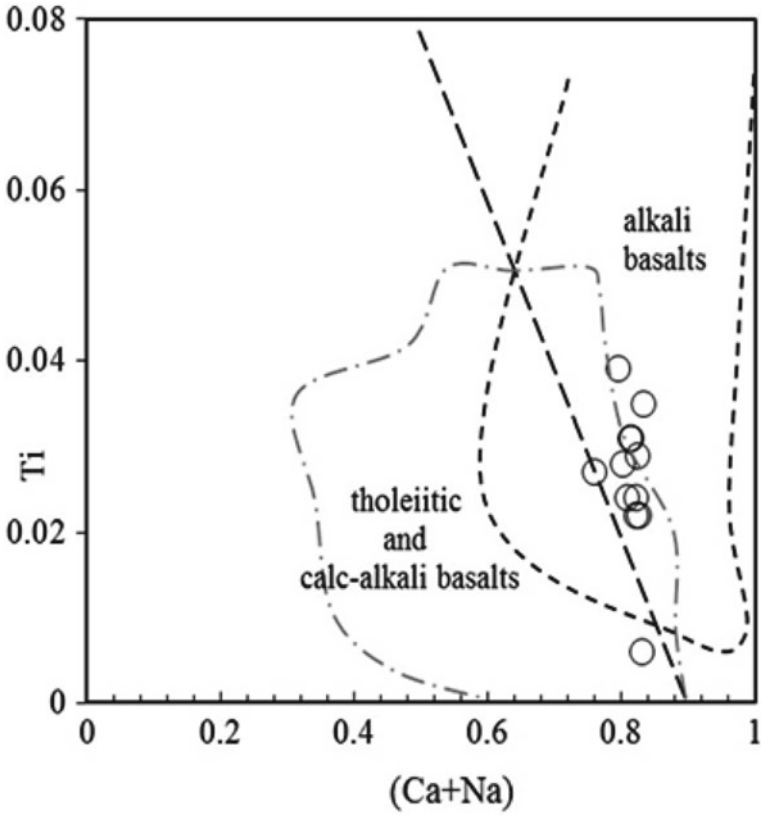


**Fig. 7** Ca + Na versus Ti binary mineral chemistry diagram for pyroxene (after Leterrier et al. 1982), showing the alkaline nature of the clinopyroxenes

2.95%, $FeO^T$ contents range from 13.13 to 17.14% and MnO contents range from 0.16 to 0.49%. The clinopyroxene is compositionally a Ti-augite ($Wo_{40}En_{34}Fs_{26}$). MgO contents vary from 9.93 to 13.53%, CaO from 17.92 to 19.90%, $Na_2O$ from 0.21 to 0.32%, maximum $K_2O$ content up to 0.14%, NiO up to 0.13% and $Cr_2O_3$ content up to 0.02%. End member calculation from the EPMA analytical data indicate variation in composition from $wollastonite_{31.60–41.61\%}$, $enstatite_{818.62–31.69\%}$ to $ferrosilite_{022.71–040.76\%}$. On the Wollastonite (Wo)-Enstatite (En)-Ferrosilite (Fs) ternary diagram, pyroxenes of the Jonnagiri porphyritic dyke fall in the field of augite, but close to the boundary of augite and diopside (Fig. 6).

The titanium concentrations in these clinopyroxenes slightly overlap with basalts derived from tholeiitic and calc-alkaline lineage (Fig. 7; Leterrier et al. 1982). However, it is observed that the pyroxenes of the Jonnagiri porphyritic dyke indicate the alkaline nature when plotted in the Ca + Na versus Ti binary mineral chemistry

diagram (after Leterrier et al. 1982). Plagioclase with andesine composition (Fig. 5) supports this observation. The mineral chemistry of the pyroxene of the Jonnagiri porphyritic dyke is presented in Table 2.

### 4.3 Fe–Ti Oxides

Notable amounts of titano-magnetite and ilmenite are noticed as euhedral to subhedral grains at the vicinity of the clinopyroxene (Figs. 3d, e, f). Both Ti-oxide and T–Fe oxide are more or less uniformly distributed in the rock. At places, Fe–Ti oxides are partially enclosed in the plagioclase laths that exhibit ophitic relation with the clinopyroxene. Exsolution intergrowth texture is conspicuously noticed in the Fe–Ti oxides. Presence of exsolved phases of Fe–Ti oxides in magmatic rocks are often associated both with the mafic intrusions and in the anorthosite massifs of Proterozoic age (Lister 1966; Haggerty and Rumble 1976; Ashwal 1982; Frost and Lindsley 1991). Titano-magnetite indicates the physical and chemical conditions of the mafic intrusions during their crystallization (e.g. Tan et al. 2016). The mineral chemistry of the ilmenite and titano-magnetite from the Jonnagiri porphyritic dyke is presented in Table 3.

EPMA data of ilmenite (FeO $TiO_2$) indicate that $TiO_2$ contents range from 46.07 to 49.71%, and $FeO^T$ contents range from 46.17 to 46.44%. $Cr_2O_3$ content up to 0.53% has been recorded, while a maximum NiO content up to 0.11% has been observed. End member calculation from the EPMA analytical data indicate variation between $ilmenite_{87.64–92.46\%}$, $geikelite_{0.008–0.075\%}$, $pyrophanite_{3.82–4.40\%}$, and $hematite_{3.60–7.93\%}$.

EPMA composition of titano-magnetite (FeO $Fe_2O_3$ $TiO_2$) indicate that the $FeO^T$ contents range from 79.39 to 79.62% and $TiO_2$ from 11.53 to 12.1%. MnO content range from 0.42 to 0.50%, while $Cr_2O_3$ content up to 0.15% and NiO content up to 0.04%. BSE images indicate that at places both ilmenite and titano-magnetite are noticed in continuity; and in such places ilmenite is noticed in the core, while titano-magnetite occurs at the peripheral parts of the ilmenite (Fig. 4a). End member calculation from EPMA analytical data indicate that their composition from $ilmenite_{21.54–22.69\%}$, geikelite up $to_{0.13\ \%}$, $pyrophanite_{0.95–1.23\%}$, to $hematite_{76.05–77.35\ \%}$.

### 4.4 Apatite

Apatite is a conspicuous accessory phase and found to be associated with clinopyroxene. Euhedral apatite is often noticed as inclusions within the clinopyroxene (Fig. 4b). EPMA data indicate CaO content up to 53.94% and $P_2O_5$ content up to 40.31 for the apatite inclusions in clinopyroxenes.

**Table 2** Mineral chemistry of clinopyroxene from the porphyritic dyke, Jonnagiri schist belt, EDC, India

| Point no. | 3 | 4 | 8 | 9 | 11 | 12 | 15 | 16 | 23 | 24 | 25 | 26 |
|---|---|---|---|---|---|---|---|---|---|---|---|---|
| $SiO_2$ | 49.724 | 49.488 | 49.713 | 49.764 | 49.821 | 49.194 | 49.629 | 49.542 | 49.488 | 49.680 | 48.087 | 49.127 |
| $TiO_2$ | 0.744 | 1.229 | 0.963 | 0.743 | 0.938 | 1.065 | 1.015 | 0.836 | 1.054 | 0.812 | 0.183 | 1.336 |
| $Al_2O_3$ | 1.396 | 2.158 | 1.831 | 1.328 | 1.904 | 2.004 | 1.957 | 1.599 | 1.970 | 1.523 | 0.354 | 2.950 |
| $Cr_2O_3$ | 0.000 | 0.014 | 0.020 | 0.006 | 0.000 | 0.017 | 0.009 | 0.007 | 0.000 | 0.000 | 0.019 | 0.019 |
| FeOT | 16.551 | 13.224 | 13.765 | 17.090 | 13.611 | 15.570 | 15.288 | 17.141 | 15.983 | 17.144 | 23.556 | 13.132 |
| MnO | 0.423 | 0.162 | 0.343 | 0.496 | 0.359 | 0.366 | 0.427 | 0.328 | 0.376 | 0.498 | 0.475 | 0.401 |
| MgO | 10.399 | 12.561 | 12.417 | 9.993 | 13.539 | 11.173 | 11.073 | 10.412 | 10.768 | 10.251 | 6.163 | 12.346 |
| CaO | 19.255 | 19.906 | 18.913 | 19.266 | 17.929 | 19.143 | 19.451 | 18.950 | 19.046 | 19.334 | 18.690 | 18.787 |
| $Na_2O$ | 0.220 | 0.254 | 0.294 | 0.308 | 0.324 | 0.322 | 0.296 | 0.253 | 0.302 | 0.296 | 0.216 | 0.290 |
| K2O | 0.007 | 0.006 | 0.000 | 0.000 | 0.012 | 0.000 | 0.006 | 0.000 | 0.000 | 0.010 | 0.014 | 0.000 |
| NiO | 0.000 | 0.044 | 0.000 | 0.132 | 0.000 | 0.069 | 0.000 | 0.016 | 0.000 | 0.014 | 0.000 | 0.000 |
| Total | 98.722 | 99.085 | 98.259 | 99.145 | 98.442 | 98.987 | 99.163 | 99.084 | 98.987 | 99.562 | 97.758 | 98.389 |
| $Fe_2O_3$ | 1.224 | 2.490 | 1.702 | 1.636 | 2.447 | 2.403 | 1.683 | 1.678 | 1.376 | 2.194 | 2.611 | 1.129 |
| FeO | 15.449 | 10.983 | 12.234 | 15.618 | 11.409 | 13.408 | 13.773 | 15.631 | 14.745 | 15.169 | 21.206 | 12.116 |
| Total | 98.842 | 99.295 | 98.429 | 99.290 | 98.682 | 99.164 | 99.320 | 99.252 | 99.125 | 99.782 | 98.019 | 98.501 |
| Cations: | 6(O) | 6(O) | 6(O) | 6(O) | 6(O) | 6(O) | 6(O) | 6(O) | 6(O) | 6(O) | 6(O) | 6(O) |
| Si | 1.937 | 1.890 | 1.916 | 1.935 | 1.907 | 1.900 | 1.913 | 1.924 | 1.916 | 1.921 | 1.955 | 1.889 |
| Ti | 0.022 | 0.035 | 0.028 | 0.022 | 0.027 | 0.031 | 0.029 | 0.024 | 0.031 | 0.024 | 0.006 | 0.039 |

(continued)

**Table 2** (continued)

| Point no. | 3 | 4 | 8 | 9 | 11 | 12 | 15 | 16 | 23 | 24 | 25 | 26 |
|---|---|---|---|---|---|---|---|---|---|---|---|---|
| Al | 0.064 | 0.097 | 0.083 | 0.061 | 0.086 | 0.091 | 0.089 | 0.073 | 0.090 | 0.069 | 0.017 | 0.134 |
| Cr | 0.000 | 0.000 | 0.001 | 0.000 | 0.000 | 0.001 | 0.000 | 0.000 | 0.000 | 0.000 | 0.001 | 0.001 |
| $Fe^{+3}$ | 0.036 | 0.072 | 0.049 | 0.048 | 0.070 | 0.070 | 0.049 | 0.049 | 0.040 | 0.064 | 0.080 | 0.033 |
| $Fe^{+2}$ | 0.503 | 0.351 | 0.394 | 0.508 | 0.365 | 0.433 | 0.444 | 0.508 | 0.477 | 0.491 | 0.721 | 0.390 |
| Mn | 0.014 | 0.005 | 0.011 | 0.016 | 0.012 | 0.012 | 0.014 | 0.011 | 0.012 | 0.016 | 0.016 | 0.013 |
| Mg | 0.604 | 0.715 | 0.714 | 0.579 | 0.773 | 0.643 | 0.636 | 0.603 | 0.621 | 0.591 | 0.373 | 0.708 |
| Ca | 0.804 | 0.814 | 0.781 | 0.803 | 0.735 | 0.792 | 0.803 | 0.789 | 0.790 | 0.801 | 0.814 | 0.774 |
| Na | 0.017 | 0.019 | 0.022 | 0.023 | 0.024 | 0.024 | 0.022 | 0.019 | 0.023 | 0.022 | 0.017 | 0.022 |
| K | 0.000 | 0.000 | 0.000 | 0.000 | 0.001 | 0.000 | 0.000 | 0.000 | 0.000 | 0.000 | 0.001 | 0.000 |
| Ni | 0.000 | 0.001 | 0.000 | 0.004 | 0.000 | 0.002 | 0.000 | 0.000 | 0.000 | 0.000 | 0.000 | 0.000 |
| Total | 4.000 | 4.000 | 4.000 | 4.000 | 4.000 | 4.000 | 4.000 | 4.000 | 4.000 | 4.000 | 4.000 | 4.000 |
| Wollastonite | 40.990 | 41.618 | 40.068 | 41.079 | 37.609 | 40.618 | 41.274 | 40.256 | 40.698 | 40.815 | 40.608 | 40.376 |
| Enstatite | 30.798 | 36.535 | 36.597 | 29.643 | 39.511 | 32.982 | 32.689 | 30.772 | 32.011 | 30.106 | 18.629 | 36.914 |
| Ferrosilite | 28.212 | 21.847 | 23.335 | 29.278 | 22.880 | 26.400 | 26.037 | 28.972 | 27.292 | 29.079 | 40.763 | 22.710 |

**Table 3** Mineral chemistry of ilmenite and titano-magnetite from the porphyritic dyke, Jonnagiri schist belt, EDC, India

| | EPMA analyses of ilmenite | | | | | EPMA analyses of titano-magnetite | | |
|---|---|---|---|---|---|---|---|---|
| | 14/1 | 19/1 | 25/1 | 29/1 | 30/1 | 15/1 | 24/1 | 31/1 |
| $SiO_2$ | 0 | 0.016 | 0.049 | 0.029 | 0.02 | 0.207 | 0.046 | 0.051 |
| $TiO_2$ | 46.207 | 49.716 | 46.368 | 46.076 | 46.241 | 12.169 | 11.615 | 11.538 |
| $Al_2O_3$ | 0.005 | 0.024 | 0.005 | 0 | 0.002 | 0.036 | 0.682 | 0.03 |
| $Cr_2O_3$ | 0.027 | 0 | 0.053 | 0.037 | 0.012 | 0.076 | 0.106 | 0.151 |
| FeOT | 46.314 | 46.173 | 46.448 | 46.208 | 46.357 | 79.629 | 78.394 | 79.48 |
| MnO | 1.817 | 1.75 | 1.925 | 1.943 | 1.889 | 0.505 | 0.421 | 0.494 |
| MgO | 0.002 | 0.026 | 0.019 | 0.005 | 0.003 | 0.034 | 0.008 | 0 |
| CaO | 0.012 | 0 | 0.028 | 0.133 | 0.086 | 0.144 | 0.027 | 0.016 |
| $Na_2O$ | 0.004 | 0 | 0.002 | 0 | 0 | 0.011 | 0.027 | 0.031 |
| $K_2O$ | 0.013 | 0.005 | 0.001 | 0.029 | 0.035 | 0.001 | 0 | 0.019 |
| NiO | 0 | 0.065 | 0.014 | 0.111 | 0.072 | 0.044 | 0 | 0 |
| Total | 94.401 | 97.775 | 94.912 | 94.571 | 94.717 | 92.856 | 91.326 | 91.81 |
| $Fe_2O_3$ | 7.423 | 3.715 | 7.488 | 7.870 | 7.730 | 77.004 | 76.118 | 77.531 |
| FeO | 39.634 | 42.830 | 39.710 | 39.126 | 39.401 | 10.338 | 9.899 | 9.714 |
| Total | 95.144 | 98.147 | 95.662 | 95.359 | 95.491 | 100.568 | 98.949 | 99.575 |
| Cations: | 3(O) | 3(O) | 3(O) | 3(O) | 3(O) | 3(O) | 3(O) | 3(O) |
| Si | 0.000 | 0.000 | 0.001 | 0.001 | 0.001 | 0.005 | 0.001 | 0.001 |

(continued)

**Table 3** (continued)

| | EPMA analyses of ilmenite | | | | | EPMA analyses of titano-magnetite | | |
|---|---|---|---|---|---|---|---|---|
| | 14/1 | 19/1 | 25/1 | 29/1 | 30/1 | 15/1 | 24/1 | 31/1 |
| Ti | 0.926 | 0.963 | 0.924 | 0.921 | 0.923 | 0.238 | 0.231 | 0.229 |
| Al | 0.000 | 0.001 | 0.000 | 0.000 | 0.000 | 0.001 | 0.021 | 0.001 |
| Cr | 0.001 | 0.000 | 0.001 | 0.001 | 0.000 | 0.002 | 0.002 | 0.003 |
| $Fe^{+3}$ | 0.149 | 0.072 | 0.149 | 0.157 | 0.154 | 1.510 | 1.514 | 1.538 |
| $Fe^{+2}$ | 0.883 | 0.923 | 0.880 | 0.869 | 0.874 | 0.225 | 0.219 | 0.214 |
| Mn | 0.041 | 0.038 | 0.043 | 0.044 | 0.042 | 0.011 | 0.009 | 0.011 |
| Mg | 0.000 | 0.001 | 0.001 | 0.000 | 0.000 | 0.001 | 0.000 | 0.000 |
| Ca | 0.000 | 0.000 | 0.001 | 0.004 | 0.002 | 0.004 | 0.001 | 0.000 |
| Na | 0.000 | 0.000 | 0.000 | 0.000 | 0.000 | 0.001 | 0.001 | 0.002 |
| K | 0.000 | 0.000 | 0.000 | 0.001 | 0.001 | 0.000 | 0.000 | 0.001 |
| Ni | 0.000 | 0.001 | 0.000 | 0.002 | 0.002 | 0.001 | 0.000 | 0.000 |
| Ilmenite | 88.434 | 92.465 | 88.122 | 87.641 | 87.954 | 22.693 | 22.203 | 21.541 |
| Geikelite | 0.008 | 0.100 | 0.075 | 0.020 | 0.012 | 0.133 | 0.032 | 0.000 |
| Pyrophanite | 4.106 | 3.827 | 4.327 | 4.408 | 4.271 | 1.123 | 0.956 | 1.109 |
| Hematite | 7.452 | 3.609 | 7.476 | 7.931 | 7.763 | 76.051 | 76.809 | 77.350 |

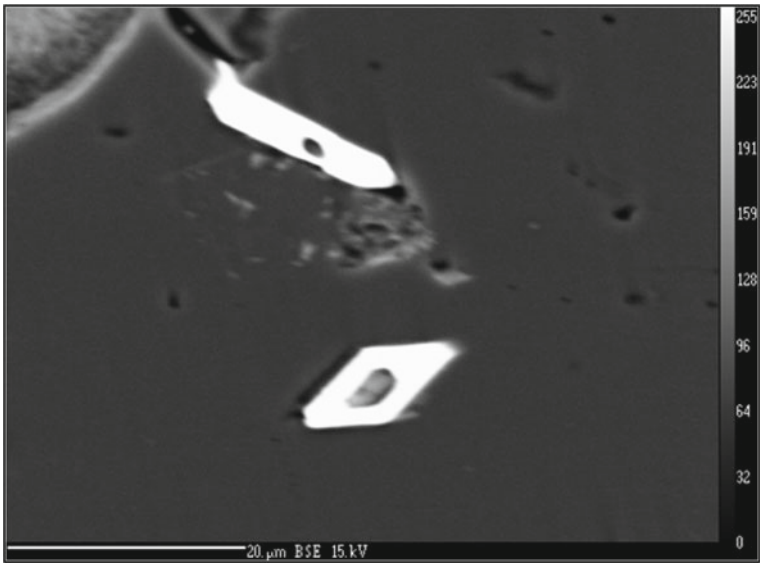


**Fig. 8** BSE image showing the euhedral nature of the micron size baddeleyite grains in the Jonnagiri porphyritic dyke

### *4.5 Baddeleyite*

The baddeleyite grains show alignment and at places partially transect ilmenite grains (Fig. 4c). BSE image shows euhedral nature of baddeleyite (Fig. 8). Due to the high uranium and minimal initial lead contents, baddeleyite ($ZrO_2$) occur as accessory phase in mafic rocks and is considered to be a reliable geochronometer (Smith 2010). However, baddeleyite in Jonnagiri porphyritic dyke occur as minute grains ranging in size from 10 to 12 μm.

## 5 Discussions

The present study deals with plagioclase megacrysts bearing porphyritic mafic dyke from the Jonnagiri greenstone belt, in EDC, Southern India. The plagioclase phenocrysts in the Jonnagiri porphyritic dyke range in size from 0.5 to 3.2 cm. Field and megascopic studies indicate that the euhedral plagioclase phenocrysts with well preserve terminal ends indicate the undeformed nature and presence of primary magmatic alignment in the Jonnagiri porphyritic dyke. Partial resorption in some plagioclase phenocryst indicates crystal—melt interaction. Alignment of plagioclase phenocrysts in mafic dykes has been described as a feature resulting due to flow differentiation (e.g. Ross 1986). Increase in phenocryst groundmass from the centre

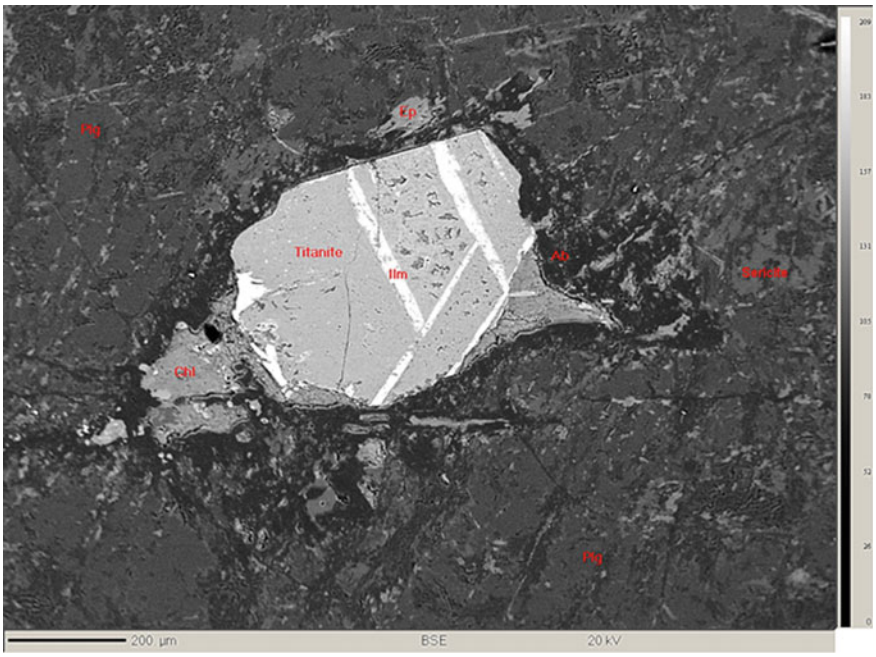


**Fig. 9** BSE image showing exsolved ilmenite in titanite inclusion in plagioclase megacryst in the Jonnagiri porphyritic dyke

to the peripheral parts in porphyritic dyke has been explained in terms of increase in the velocity gradient and the fluid viscosity (e.g. Komar 1972). Euhedral plagioclase megacrysts of 2–5 cm size have been recorded in the Tarssartoq dyke swarm to the north of Isua Greenstone belt of Greenland (White et al. 2000). The larger plagioclase phenocrysts confined to the central part of the dyke crystallize when the magma resides at relatively deeper level and the groundmass phases crystallize when the magma is emplaced to sub crustal levels. Presence of sub-ophitic/ophitic textures in Jonnagiri porphyritic dyke (Figs. 3b, c) substantiate the magmatic origin. Ophitic/sub-ophitic textures in coarse grained dykes contain magmatic pyroxene (e.g. White et al. 2000). Exsolution textures in the form of ilmenite and titanomagnetite intergrowth conspicuously noticed in the Jonnagiri porphyritic dyke also support the magmatic origin. Fe and Ti enriched melts crystallize abundant titanomagnetite at an early stage (e.g. Pang et al. 2008). Partially enclosed euhedral to subhedral opaques in the ophitic plagioclase lath (Fig. 3c) and clinopyroxene (Fig. 3e) indicate early crystallisation of the Fe–Ti oxides in the Jonnagiri porphyritic dyke. Notable variation both in the abundance and size of plagioclase phenocrysts can be noticed in outcrop scale in the megacrystic plagioclase bearing amphibolites in Flekkefjord area, South Norway (Falkum and Grundvig 2001). The size of the plagioclase megacrysts from gabbroic dykes in the Gardar Province vary from <1 cm to 1 m (Halama et al. 2002). Low degree alkaline nature is evidenced by the presence of plagioclase phenocryst

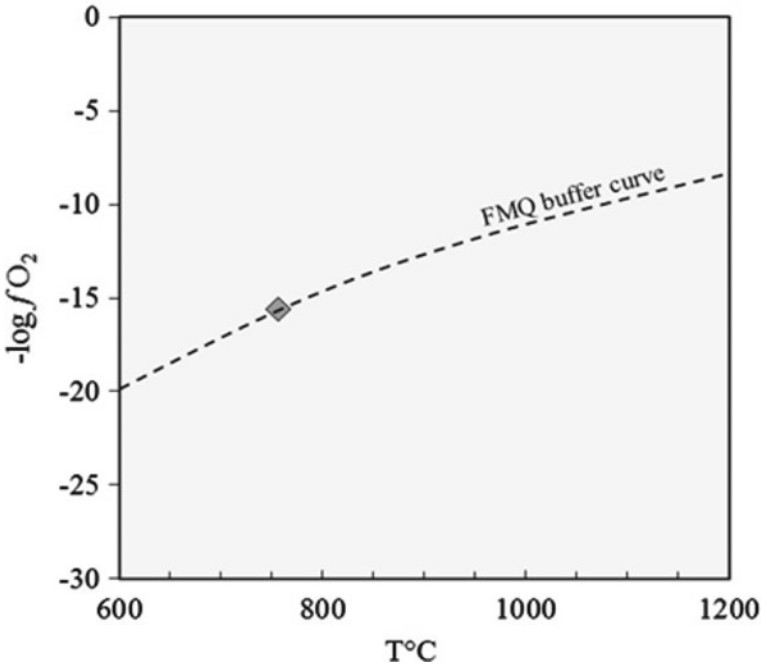


**Fig. 10** Binary plot showing temperature and oxygen fugacity estimates for the coexisting magnetite-ilmenite solid solution pairs Lepage (2014). FMQ curve in the figure is after Frost (1991)

with composition varying from andesine to labradorite composition in the porphyritic mafic dyke from the Jonnagiri greenstone belt. Mafic dykes with low degree alkaline, transitional to tholeiitic character have been reported in a continental tectonic from the Izera Complex, West Sudetes, Poland (Ilnicki 2010).

Microprobe analyses of plagioclase grains in the Jonnagiri porphyritic dyke indicate the presence of zoning phenomenon. The core analysed $Na_2O$ content of 5.16% and CaO content of 10.01%, while the rim analysed $Na_2O$ content of 5.64% and CaO content of 9.32% (Table 2). Increase in Na ($Ab_{45.73}$ to $Ab_{49.61}$) and decrease in Ca ($An_{49.01}$ to $An_{45.34}$) from core to rim indicate normal zoning in the plagioclase, a characteristic feature indicating relatively high temperature in core and lower temperature in the rim resulted from crystallisation of magma. Further presence of exsolved ilmenite within the titanite inclusion in the plagioclase megacryst (Fig. 9) affirm the magmatic origin for the dyke.

Alteration studies on granites indicated replacement of titanite by ilmenite (e.g. Broska et al. 2007), however, implications of exsolved ilmenite in titanite inclusion in the plagioclase megacrysts in mafic dykes is less understood. It is notable that composition of most of the plagioclase grains in Jonnagiri porphyritic dyke are predominantly andesine. Wyers and Barton (1986) have reported transitional lavas of alkaline—sub-alkaline composition from the Patmos province in Greece. The

predominantly andesine composition of plagioclase grains, position of the clinopyroxene in the Ca + Na versus Ti binary mineral chemistry diagram (after Leterrier et al. 1982), and micro size euhedral baddeleyite grains indicate the transitional nature of the Jonnagiri porphyritic dyke that is presumably emplaced in a rift related setting. However, detailed geochemical and geochronological studies are the gap areas that can be taken up for further research.

The temperature and oxygen fugacity estimates for the coexisting magnetite-ilmenite solid solution pairs using the calculation software given by Lepage (2014) yielded an equilibration temperature of ~756 °C and $10^{-15.6}$atm$f_{O2}$. The equilibrium conditions are consistent with an oxide equilibration path defined by a fayalite-magnetite-quartz (FMQ) buffer curve (Fig. 10; Frost 1991). The basaltic rocks generated in arc settings are commonly characterized by oxygen fugacities necessarily more oxidizing than the FMQ buffer ($10^{-8}$–$10^{-3}$) at a given temperature (1200 °C; cf. Frost 1991). The estimate for the Jonnagiri dyke is consistent with a relatively non-oxidizing i.e. reducing environment.

## 6 Conclusions

The porphyritic mafic dyke from the Jonnagiri greenstone belt described in the present study is characterised by presence of euhedral plagioclase megacrysts showing magmatic alignment. Partially resorbed plagioclase phenocryst indicates crystal-melt interaction. Petrographically Jonnagiri dyke exhibits porphyritic texture with magmatically aligned plagioclase phenocrysts set in groundmass andesine and titan augite. Fe–Ti oxides; ilmenite and titano-magnetite exhibiting exsolved textures are notable, while apatite and baddeleyite are the accessory phases. The predominant andesine compositions of the plagioclase grains indicate transitional nature of the Jonnagiri porphyritic dyke. The temperature and oxygen fugacity estimates for the coexisting magnetite-ilmenite solid solution pairs yielded an equilibration temperature of ~756 °C and $10^{-15.6}$atm$f_{O2}$.

**Acknowledgements** The Director General, Geological Survey of India, is thankfully acknowledged, for providing an opportunity to work in the field area as part of the GSI-Geoscience Australia field workshop in March 2017. Additional Director General and HOD, Geological Survey of India, Southern Region, Hyderabad is thanked for his kind support. Michael Doublier, Geoscience Australia, is profusely thanked for helpful discussions during a field Workshop in Jonnagiri schist belt. M. L. Dora and Jeff Karson are profusely thanked for critical and constructive review. Editorial comments of Rajesh K. Srivastava have also helped to improve the MS. VVSS and SB thanks Pravir Pankaj, GSI, for the support in the field.

## References

Ashwal LD (1982) Mineralogy of mafic and Fe–Ti oxide rich differentiates of the Marcy anorthosite massif, Adirondacks, New York. Am Mineral 67:14–27

Belica ME, Piispa EJ, Meert JG, Pesonen LJ, Plado J, Pandit MK, Kamenov GD, Celestino M (2013) Paleoproterozoic mafic dyke swarms from the Dharwar craton; palaeomagnetic poles for India from 2.37 to 1.88 Ga and rethinking the Columbia supercontinent. Precambr Res 244:100–122

Broska I, Harlov D, Tropper P, Siman P (2007) Formation of magmatic titanite and titanite-ilmenite phase relations during granite alteration in the Tribec Mountains, western carpathians, Slovakia. Lithos 95:58–71

Dora ML, Mahapatro SN, Singh H, Malaviya VP, Shareef M, Wankhade SH, Ranadive K (2016) Plagioclase Megacrysts in Proterozoic Leucogabbronorite Dyke from Bastar Craton, Central India: Melt-crystal interaction at crustal level. Paper presented at the 35th international geological congress, Cape Town, South Africa, 27th August–4th September 2016

Falkum T, Grundvig S (2001) Origin of plagioclase-megacrystic, orthopyroxene amphibolites within a Precambrian banded gneiss suite, Flekkefjord area Vest-Agder, South Norway. NGU Bull 438:5

Frost BR (1991) Magnetic petrology: factors that control the occurrence of magnetite in crustal rocks. Rev Miner Geochem 25:489–509

Frost BR, Lindsley DH (1991) Occurrence of iron-titanium oxides in igneous rocks. oxide minerals: petrologic and magnetic significance. Miner Soc Am, Rev Miner 25:433–468

Haggerty SE, Rumble D (1976) Opaque mineral oxides in terrestrial igneous rocks. Oxide Miner: Miner Soc Am, Rev Miner 3:Hg101–Hg300

Halama R, Waight T, Markl G (2002) Geochemical and isotopic zoning patterns of plagioclase megacrysts in gabbroic dykes from the Gardar Province, South Greenland: implications for crystallisation processes in anorthositic magmas. Contrib Mineral Petrol 144(1):109–127

Halls HC, Kumar A, Srinivasan R, Hamilton MA (2007) Palaeomagnetism and U–Pb geochronology of eastern trending dykes in the Dharwar craton, India: feldspar clouding, radiating dyke swarms and position of India at 2.37 Ga. Precambr Res 155:47–68

Hou GT, Santosh M, Xianglin Qian GS, Li JH (2008) Configuration of the Late Paleoproterozoic supercontinent Columbia: insights from radiating mafic dyke swarms. Gondwana Res 14:395–409

Ilnicki S (2010) Petrogenesis of continental mafic dykes from the Izera Complex, Karkonosze-Izera Block (West Sudetes, SW Poland). Int J Earth Sci 99(4):745–773

Jairam MS, Roop Kumar D, Srinivasan KN (2001) Classification of greenstones and associated granitoids of Jonnagiri schist belt, Kurnool District, Andhra Pradesh. Geol Surv India Spec Pub 55:59–66

Jayananda M, Mahesha N, Srivastava RK, Blais S (2008) Petrology and geochemistry of Paleoproterozoic high-magnesian norite and dolerite dyke swarms from the Halagur-Satnur areas, Eastern Dharwar Craton, Southern India. In: Srivastava RK, Sivaji C, Chalapathi Rao NV (eds) Indian Dykes: Geochemistry, Geophysics and Geochronology. Narosa Publishing House Pvt. Ltd., New Delhi, pp 239–260

Khanna TC, Sesha Sai VV, Zhao GC, Subba Rao DV, Keshav Krishna A, Sawant SS, Charan SN (2013) Petrogenesis of mafic alkaline dikes from the ~2.18 Ga Mahbubnagar Large Igneous Province, Eastern Dharwar Craton, India: geochemical evidence for uncontaminated intra continental mantle derived magmatism. Lithos 179:84–98

Komar PD (1972) Mechanical interactions of phenocrysts and flow differentiation of igneous dikes and sills. Geol Soc Am Bull 83(4):973–988

Kumar A, Nagaraju E, Besse J, Bhaskar Rao YJ (2012) New age, geochemical and palaeomagnetic data on a 2.21 Ga dyke swarm from south India: constraints on Paleoproterozoic reconstruction. Precambr Res 220:123–138

Kumar A, Parashuramulu V, Nagaraju E (2015) A 2082 Ma radiating dyke swarm in the Eastern Dharwar Craton, southern India and its implications to Cuddapah basin formation. Precambr Res 266:490–505

Lepage DL (2014) ILMAT: A magnetite-Ilmenite Geothermobarometry Program (version 1.20c)

Leterrier J, Maury RC, Thonon P, Girard D, Marchal M (1982) Clinopyroxene composition as a method of identification of the magmatic affinities of paleo-volcanic series. Earth Planet Sci Lett 59:139–154

Lister GF (1966) The composition and origin of selected iron–titanium deposits. Econ Geol 61:275–310

Manikyamba C, Ganguly S, Santosh M, Singh RM, Saha A (2015) Arc-nascent back-arc signatures in metabasalts from the neoarchaean Jonnagiri greenstone terrane, Eastern Dharwar Craton, India. Geol J 50:651–669

Morrison DA, Phinney WC, Maczuga DE (1988) The Petrogenetic significance of plagioclase megacrysts in Archean rocks. Lunar and Planetary Inst., Workshop on the Deep Continental Crust of South India, pp 112–114

Naqvi SM, Rogers JJW (1987) Precambrian geology of India, Oxford Monographs on Geology and Geophysics. Oxford University Press, Oxford, p 223

Pang KN, Zhou MF, Lindsley D, Zhao D, Malpas J (2008) Origin of Fe–Ti oxide ores in mafic intrusions: evidence from the Panzhihua Intrusion, SW China. J Petrol 49(2):295–313

Phinney WC, Morrison DA (1986) Petrogenesis of calcic plagioclase megacrysts in Archean rocks. Lunar and Planetary Inst. Workshop on Early Crustal Genesis: The World's Oldest Rocks p 90–91

Piispa EJ, Smirnov AV, Pesonen LJ, Lingadevaru M, Anantha Murthy KS, Devaraju TC (2011) An integrated study of proterozoic dykes, Dharwar Craton, Southern India. In: Srivastava RK (ed) Dyke Swarms: Keys for Geodynamic Interpretation. Springer, New York, pp 33–45

Radhakrishna BP (2008) Foreword—Precambrian mafic magmatism in Indian shield. J Geol Soc India 72:5

Radhakrishna T, Joseph M (1996) Proterozoic palaeomagnetism of the mafic dyke swarms in the high grade region of south India. Precambr Res 76:31–46

Ross ME (1986) Flow differentiation, phenocryst alignment, and compositional trends within a dolerite dike at rockport, Massachusetts. Bull Geol Soc Am 97(2):232–240

Santosh M (2012) India's Paleoproterozoic legacy. In: Mazumder R, Saha D (eds) Paleoproterozoic of India: geological society, Special Publications, London, vol. 365, pp 263–288

Sesha Sai VV, Tripathy V, Bhattacharjee S, Khanna TC (2017) Paleoproterozoic magmatism in the Cuddapah basin India. J Indian Geophys Union 21(6):516–525

Smith KF (2010) Potential for baddeleyite in U–Pb dating of mafic alkaline rocks from the Balcones Igneous Province, Texas. In Session No. 277. Recent Advances in Mineralogy and Petrology. Presented at the annual meeting of the Geological Society of America, Denver, vol 42(5), p 647

Sreeramachandra Rao K, Roop Kumar D, Jairam MS, Bhattacharjee S, Ananda Murthy S, Krishna Rao PV (2001) Interpretation of geological characteristic of Dona gold prospect, Jonnagiri schist belt, Kurnool district, Andhra Pradesh. Geol Surv India Spec Pub 58:217–231

Srivastava RK (ed) (2011) Dyke Swarms: keys for geodynamic interpretations, Springer, ISBN 978-3-642-12496-9

Srivastava RK, Ahmed T (2009) Precambrian mafic magmatism in the Indian shield: retrospect and prospect. J Geol Soc India 73(1):7–11

Srivastava RK, Sivaji C, Chalapathi Rao NV (eds) (2008) Indian dykes through space and time: retrospect and prospect. Geochemistry, Geophysics and Geochronology, Narosa Publishing House Pvt. Ltd., New Delhi, Indian Dykes, pp 1–18

Srivastava RK, Kumar S, Sinha AK, Chalapathi Rao NV (2014a) Petrology and geochemistry of high titanium and low titanium mafic dyes from the Damodar Valley, Chottanagpur Gneissic terrain, eastern India and their relation to Cretaceous mantle plumes (s). J Asian Earth Sci 84:34–50

Srivastava RK, Jayananda M, Gautam GC, Gireesh V, Samal AK (2014b) Geochemistry of an ENE–WSW to NE–SW trending ~2.37 Ga mafic dyke swarm of the eastern Dharwar craton, India: does it represent a single magmatic event? Chemie der Erde Geochemistry 74:251–265

Srivastava RK, Jayananda M, Gautam GC, Samal AK (2014c) Geochemical studies and petrogenesis of ~2.21–2.22 Ga Kunigal mafic dyke swarm (trending N–S to NNW–SSE) from eastern Dharwar craton, India: implications for Paleoproterozoic large igneous provinces and supercraton superia. Miner Pet 108:695–711

Srivastava RK, Samal A, Gautam GC (2015) Geochemical characteristics and petrogenesis of four Palaeoproterozoic mafic dike swarms and associated large igneous provinces from the eastern Dharwar craton, India. Int Geol Rev 57(11–12):1462–1484

Suresh G, Jaiswal N (2003) Specialised thematic Mapping of the southern extension of Jonnagiri schist belt, Julakalva schist belt and adjoining granitoids of Peninsular Gneissic Complex. Rec Geol Surv India 136(5):11–12

Suresh G, Viswanatha Rao N (1994) Study of granitoids of Gooty—Singanamala area, Anantapur district. Rec Geol Surv India 128(5):376–377

Tan W, Peng L, He H, Wang YC, Liang X (2016) Mineralogy and origin of exsolution in Ti-rich magnetite from different magmatic Fe–Ti oxide-bearing intrusions. Can Miner 54(3):539–553

White RV, Crowley JL, Myers JS (2000) Earth's oldest well-preserved mafic dyke swarms in the vicinity of the Isua greenstone belt, southern West Greenland. Geol Greenl Surv Bull 186:65–72

Wyers PG, Barton M (1986) Petrology and evolution of transitional alkaline - sub alkaline lavas from Patmos, Dodecanesos, Greece: evidence for fractional crystallization, magma mixing and assimilation. Contrib Miner Petrol 93(3):297–311

Zhao G, Sun M, Wilde SA, Li S (2004) A Paleo-Mesoproterozoic supercontinent: assembly, growth and breakup. Earth Sci Rev 67:91–123